iScience

CellPress
OPEN ACCESS

Article

Self-injection-locked thin-film regenerative laser amplifier

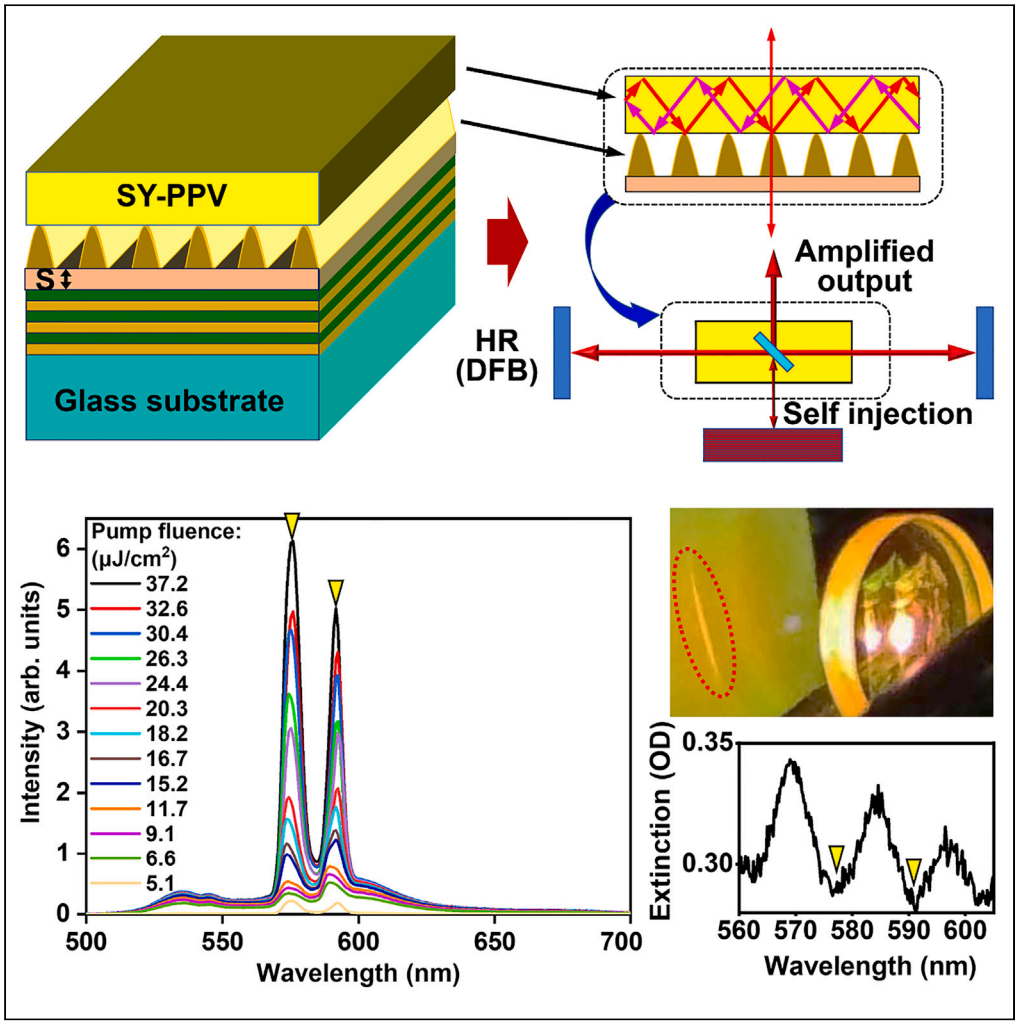

Yue Liu, Wenwen Wu, Xinping Zhang

zhangxinping@bjut.edu.cn

Highlights

A first report of a thin-film self-injection-locked regenerative laser amplifier

Observation of an exponential-growth dependence of the amplifier output on the pump

Determination of the amplified spectrum by the reflection of the Bragg reflector

A spacer layer is crucial for adjusting oscillation-amplification phase relationship

Liu et al., iScience 27, 109426
May 17, 2024
https://doi.org/10.1016/j.isci.2024.109426

iScience

CellPress
OPEN ACCESS

Article

Self-injection-locked thin-film regenerative laser amplifier

Yue Liu,[1] Wenwen Wu,[1] and Xinping Zhang[1,2,*]

SUMMARY

Organic lasers based on distributed feedback (DFB) microcavities have been extensively investigated. However, the application of these lasers is limited by their low output power and large beam divergence. Therefore, laser amplifiers are needed to achieve practically applicable laser intensity and controllable lasing modes for far-field applications. In this work, we report self-injection-locked laser amplifiers using the combination of a DFB microcavity and a Bragg reflector, where a high-reflection mirror acts as the Bragg reflector and its feedback supplies the external-cavity injection. The coherent coupling between the DFB microcavity and the Bragg amplifier is crucial for achieving high conversion efficiency and high-contrast transverse modes. An amplification factor larger than 20 and a single output laser spot with high contrast that has been achieved. Such an integration design of the self-injected DFB microcavity amplifier can be directly utilized in the realization of high-performance thin-film laser sources for practical applications.

INTRODUCTION

Thin-film polymer lasers based on photonic structures in various forms have attracted extensive research interests.[1–9] The design of such laser devices may include Fabry-perot,[3,4] whispering gallery mode,[5,6] distributed Bragg reflector (DBR),[7,8] and distributed feedback (DFB) microcavities.[10–16] The DFB microcavities are the mostly employed design for such polymer lasers, where periodic dielectric,[10–12] organic semiconductor,[13,14] or metallic[15,16] nanostructures have been used to construct the microcavities. However, most of these lasers exhibit low intensity and large divergence in their output, which limits their practical applications. Construction of injection-locked amplifiers[17–19] is one of the most effective approach to achieve laser sources with high-power, high-directionality, and high-spectral-selectivity performance. However, for such amplifiers, an additional laser is needed for supplying the injection, which not only enhances the complexity and lowers the practical applicability of such amplifiers, but also reduces the coherent interaction and conversion efficiency properties between the injection and the amplification processes. Moreover, injection locking of thin-film laser amplifier has challenges due to coupling difficulties and small interaction distance, which has been rarely reported.[20–22]

We reported in our previous publications the injection into DFB microcavities and demonstrated excellent performance of thin-film polymeric laser amplifiers.[23–25] Due to the strict conditions required by DFB microcavities, it is difficult to realize broadband tuning of the output spectrum of such amplifiers.[23] Utilization of tilted[24] or chirped[25] Bragg grating structures has been demonstrated for tuning the output spectrum of the injection-locked DFB-microcavity amplifiers. However, these are still independent schemes, where additional lasers have to be involved to supply the injection beams. In this work, we report an "independent" thin-film DFB-microcavity amplifier scheme, where the injection is supplied by the amplifier itself, so that no additional laser source is needed for the injection. Coherent coupling between the resonator and the amplifier is achieved by constructing the DFB microcavity on a Bragg reflector, where the output of the resonator is directly fed back as the injection, enabling a regenerative amplification process.

RESULTS AND DISCUSSION

Basic principles for self-injected DFB-microcavity regenerative amplifiers

Figure 1 shows the design and basic principles for the self-injected regenerative amplifier based on a DFB microcavity and a Bragg high-reflection (HR) mirror, where the DFB microcavity is realized by a photoresist (PR) grating produced by interference lithography. The HR mirror is designed for HR for a center wavelength of 532 nm and a bandwidth of about 140 nm, as shown in Figure S1. This mirror is manufactured by China Daheng Group Inc. according to the customer's required specifications. Poly(1,4-phenylene-1,2-ethenediyl) (Super yellow, SY-PPV) is employed as the gain medium of the laser and the active DFB microcavity is formed by the combination of the SY layer and the PR grating. The chemical structure of SY molecules is shown in Figure S2A and the absorption/photoluminescence (PL) spectra are given in Figure S2B. According to the microscopic characterization (as will be shown in Figure 2), the spin-coated SY layer forms a continuous and homogeneous film

[1]Institute of Information Photonics Technology, Beijing University of Technology, Beijing 100124, P.R. China
[2]Lead contact
*Correspondence: zhangxinping@bjut.edu.cn
https://doi.org/10.1016/j.isci.2024.109426

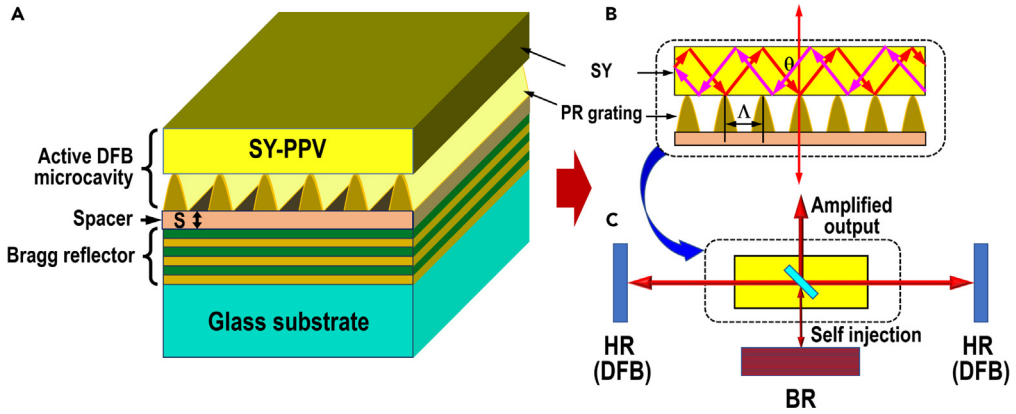

Figure 1. Basic principles for the self-injected regenerative laser amplifier using a DFB microcavity on a Bragg reflector

(A) Design of the laser amplifier device.

(B) Mechanisms for the optical feedback by input coupling through Bragg diffraction and output coupling of the DFB microcavity.

(C) The equivalent scheme by conventional discrete optics of the microcavity design in (A).

suspending on the top of the PR grating and is thus as presented in Figures 1A and 1B. A spacer layer is found necessary for adjusting the performance of the laser amplifier.

Figure 1B shows the basic principle for the DFB laser resonator. The SY layer acts both as an active layer and as a waveguide for the feedback and gain channel. The emission from the SY molecules is diffracted by the PR grating through a second-order process of

$$2n_{eff}\Lambda \sin\theta = 2\lambda, \quad \text{(Equation 1)}$$

where n_{eff} is the effective refractive index of the active DFB microcavity, Λ is the period of the PR grating, θ is the angle of incidence onto the grating, as shown in Figure 1B, and λ is the resonance wavelength of the Bragg diffraction process, which corresponds to the lasing wavelength of the DFB microcavity. The confinement and optical feedback by the microcavity are defined by the total reflection on the top surface of the SY laser and the diffraction by the PR grating on the bottom. Amplification of the molecular radiation is achieved when stimulated emission is propagating back and forth inside the SY-DFB microcavity. Lasing is produced when the gain is higher than the loss for the emission inside the microcavity.

Figure 1C explains how the self-injected amplifier works by an equivalent scheme. Lasing oscillation in the DFB microcavity is coupled out through diffraction by the PR grating into two opposite directions, as designated by the upward and downward red arrow in Figure 1B, which can be described by:

$$n_{eff}\Lambda \sin\theta = \lambda. \quad \text{(Equation 2)}$$

The HR mirrors in Figure 1C are supplied by the PR grating as a DFB microcavity and the Bragg reflection (BR) mirror supplies a nearly total back-reflection of the downward output or the injection for the amplifier, as shown by the vertical double arrow. The injection is coupled into the microcavity through the diffraction by the PR grating, using the same process as that described by Equation 2. This injection is equivalently denoted by the partial reflector inside the gain medium in Figure 1C. The injection experiences a number of the round trips inside the microcavity for amplification before being coupled into the free space (the upward arrow in Figure 1C) as the output of the amplifier.

The scheme given in Figure 1 explains our definition of this design as a regenerative amplifier. It needs to be noticed that for such an amplifier the oscillation and amplification take place simultaneously, so that the output is in fact a "mixture" that contains both the oscillation and the amplification of the laser emission. Meanwhile, the injection process not only locked the spectrum and the transverse mode of the amplifier, but also supplies an additional feedback, so that the lasing threshold is much reduced. As a result, we observed an exponential growth of the output laser intensity as a function of the pump fluence, which is completely different from that for a DFB laser oscillator with a linear dependence. All of these features actually define characteristics of such a self-injected DFB laser amplifier.

Fabrication and characterization of the devices

The PMMA spacer layer is prepared by spin-coating the PMMA/chlorobenzene solution onto the surface of the dielectric HR mirror for a center wavelength of about 560 nm. This dielectric mirror is used as the Bragg reflector in our design of the amplifier scheme, as shown in Figure 1. The thickness of the spacer layer is controlled by adjusting the spin speed while keeping constant the solution concentration.

The DFB microcavity consisting of a PR grating is fabricated by interference lithography on the top of the PMMA layer, where an ultraviolet laser at 355 nm is used as the light source. It was found that the PMMA spacer layer was not damaged by this fabrication process. In fact, there may exist a remaining PR layer between the grating structure and PMMA due to the possibly incomplete development process. In such a case, the thickness of the spacer should be a sum of that of PMMA and the remaining PR underneath the grating.

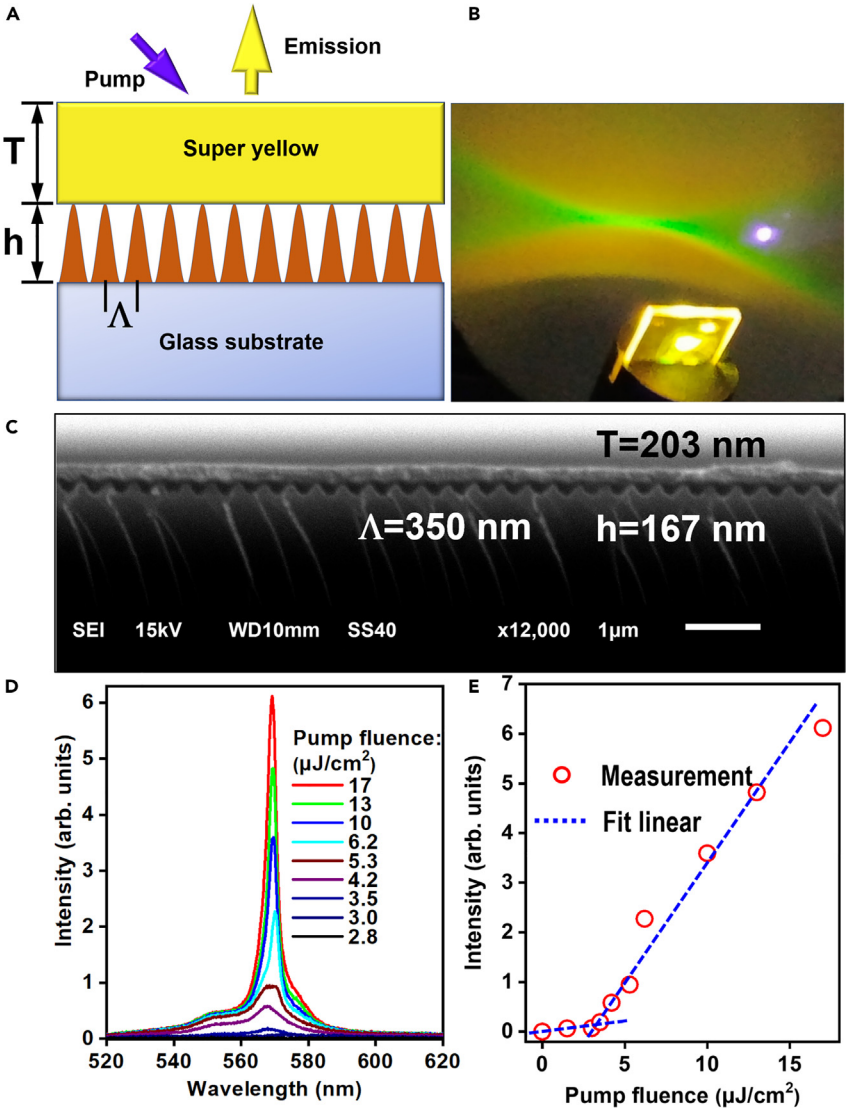

Figure 2. Design and working performance of the DFB laser oscillator

(A) Design and basic principles of the DFB-microcavity laser.

(B) Photograph of the laser device and the output laser mode.

(C) The SEM image of the cross-sectional profile of the laser device. Scale bar represents 1 μm.

(D) Lasing spectra at different pump fluences.

(E) Variation of the peak intensity of thelasing spectrum with pump fluence.

The SY-PPV solution in methylbenzene with a concentration of 5.5 mg/mL is spin-coated onto the PR grating with a speed of 1000 rpm. The concentration and the spin speed have been optimized, so that controllable thickness and excellent homogeneity of the active layer have been achieved for all fabrications. In all of the experiments, the thickness of the SY-PPV layer is about 200 nm.

In characterizing the lasing performance of both the DFB laser and the self-injected amplifier, the frequency doubled Ti:sapphire amplifier is used as the pump source, which supplies laser pulses at 400 nm with a repetition rate of 1 kHz and a pulse length of about 150 fs. The pump fluence was adjusted by a neutral attenuator with continuous tunability. The laser spectrum is acquired by an Ocean Optics spectrometer USB 4000 with a resolution of 2 nm. Output laser power is measured using a powermeter from Coherent (PM100D).

Lasing performance without injected amplification

The configuration in Figure 1A becomes a normal DFB laser without the spacer/Bragg reflector, where the DFB microcavity is sitting directly on a glass substrate, as illustrated in Figure 2A. Figure 2B is a photograph of the device and the lasing spot in green. The SEM image of the

cross-sectional profile of the device is shown in Figure 2C, which measures the SY-layer thickness of T = 203 nm, a grating period of Λ = 350 nm, and a grating modulation depth of h = 167 nm Figure 2D presents the emission spectra of the device at different pump fluence, which is increased from 2.8 to 17 $\mu J/cm^2$. A lasing peak at about 570 nm is observed when the pump fluence is higher than 3.5 $\mu J/cm^2$. The bandwidth of this lasing spectrum is about 2.7 nm at FWHM.

Figure 2E shows the variation of the peak intensity of the lasing spectrum as a function of the pump fluence. Linear fitting to the measurement data resolves two clear stages of the emission and identifies a pump threshold of about 3 $\mu J/cm^2$. A maximum average output power of 0.9 μW, or a maximum pulse energy of 0.9 nJ, was measured for this laser device at a pump fluence of about 17 $\mu J/cm^2$.

Meanwhile, the structure in Figures 2A and 2C actually shows a waveguide grating structure (WGS) with the SY-PPV waveguide suspended on the grating lines. Thus, the WGS resonance mode is clearly observed in the optical extinction spectrum, as shown in Figure S3. Figure S3A shows a comparison between optical extinction measurements on the device for transverse electric (TE) and transverse magnetic (TM) polarizations at normal incidence, where the directions of TE and TM polarizations are parallel and perpendicular to the grating lines, respectively, as shown in the inset of Figure S3A. Figure S3B shows the angle-resolved optical extinction spectrum for TE polarization as the angle of incidence is increased from 0 to 12°, where the WGS resonance mode is split into two branches tuning oppositely with the increase of the angle of incidence. For TM polarization, the WGS resonance mode is overlapped on the broadband absorption spectrum of SY-PPV, as shown in Figure S3A. However, it is not modified by the absorption spectrum for TE polarization. The surface-emitted lasing takes place at about 570 nm, as shown in Figure 2D, which is exactly the WGS resonance mode for TE at normal incidence. This also explains the mechanisms for the DFB lasing process, where the waveguide resonance mode not only satisfies the Bragg diffraction condition in Equation 1, but also supplies gain of the emission through the WGS resonance mode along the propagation in SY-PPV waveguide, which is responsible for the low pump threshold. This mechanism also applies to the self-injected amplifiers in the following sections. In fact, the optical extinction peak at 570 nm in Figure S3A roughly corresponds to the optical confinement of the incident light energy by the DFB microcavity. The peak value of optical extinction spectrum is about 0.26 OD at 570 nm, which corresponds to 45% optical confinement of the input light energy or the input coupling efficiency of the amplifier.

Self-injected regenerative laser amplification with different spacer thickness

As described previously, for the self-injected regenerative amplifier, the DFB resonator stands on a Bragg reflector, as shown in Figure 1, where a polymeric spacer layer is arranged between them. Such a spacer layer is important for improving the performance of the amplification process, which not only introduces a low-refractive index medium underneath the DFB microcavity, favoring the laser actions, but also regulates the phase shift between the injection, the oscillation, and the amplification laser beams, avoiding destructive interference between them through adjusting its thickness (S).

For S = 0, the DFB microcavity is sitting directly on the HR mirror as a Bragg reflector. Figure S4A shows the output spectra of the amplifier at different pump fluences and the inset is a photograph of the device and the lasing spot at a distance of about 6 cm from the device. This distance was also used for the experimental data in the following sections. As shown in the inset of Figure S4A, the output laser spot is green in the center and yellow on both sides. The weak green emission in the center can be understood as the direct output of the laser oscillator in the DFB microcavity without injected amplification and the bright yellow is supposed to result from the amplified injection, or in other words, the amplified injection has a "black hole" in the center. This can be attributed to the destructive interference between the injection and the regenerative amplification processes during their interactions in the normal direction.

A most notable feature in the amplification spectrum in Figure S4A is the dip at about 570 nm, which is responsible for the two-peak emission in the output laser spectrum. For understanding this, we measured the reflective optical extinction spectrum of the device, as shown in Figure S4B, where a strong modulation can be observed. The spectrum in Figure S4B is exactly the optical feedback for injection by the Bragg reflector. The dip in the lasing spectrum in Figure S4A is overlapped with one of the optical extinction peak in the reflection spectrum in Figure S4B, we highlighted by the dashed vertical line, explaining concisely the responsible mechanism for the dip feature in the lasing spectrum. Meanwhile, such spectral features with their direct correspondence verify the injection locked amplification process, where the reflection properties of the HR mirror determine the output lasing modes in both the transverse intensity distribution and the spectroscopic performance. Furthermore, a comparison between Figures 2D and S4A reveals a much broader lasing spectrum for the self-injected amplifier. Such a broadening effect can be mainly explained by both the broadband self-injection with low selectivity of the HR mirror and its close contact with the DFB resonator.

Figure S4C shows the output lasing intensity as a function of pump fluence. A maximum output average power of about 9 μW, or a maximum pulse energy of 9 nJ, is measured for a pump fluence of about 47 $\mu J/cm^2$. Two variation stages can be fitted linearly with different slopes for the lasing features peaked at about 566 and 573 nm, where the variation has a larger slope at 573 than at 566 nm for the lasing processes. Such a lasing characteristics is related to the simultaneous output from that oscillation and amplification processes. The injection-locked amplification also exhibits a threshold effect, where the injection should first overcome the input coupling loss. The amplification becomes dominant only when the injection exceeds the loss during input coupling.

Although we can measure the absolute amplification factor by:

$$\eta_A = \frac{P_A}{P_0}, \qquad \text{(Equation 3)}$$

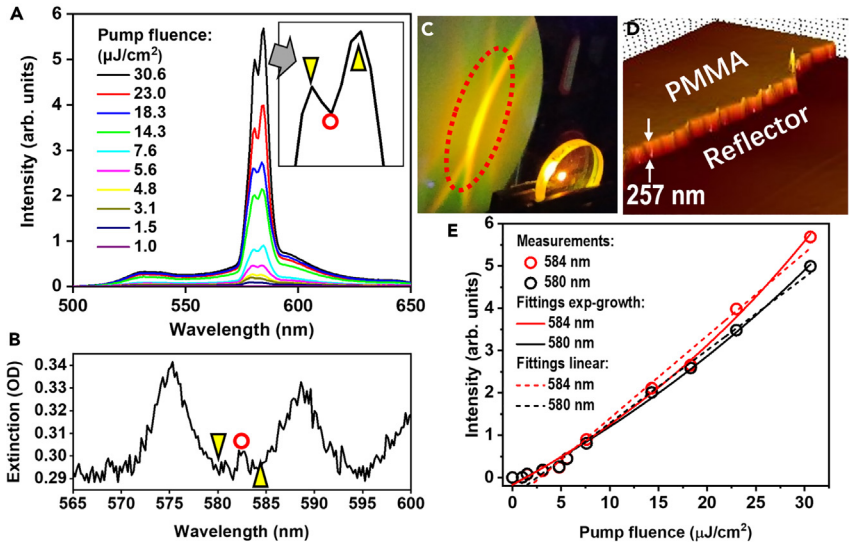

Figure 3. Self-injected regenerative laser amplification for S = 257 nm

(A) Lasing spectra of the self-injected amplifier at different pump fluences. Inset: typical spectral features.

(B) Reflection optical extinction spectrum measured on the self-injected laser amplifier on a Bragg reflector. The peak and dip features in the lasing spectra may find their correspondence in optical extinction spectrum as highlighted by the red circle and yellow triangles.

(C) Photograph of the laser and amplifier device with the output lasing spot.

(D) A three-dimensional profile image measured on the PMMA film as a spacer layer, showing a PMMA thickness of 257 nm.

(E) Measured lasing intensity as a function of pump fluence at about 580 and 584 nm, and fittings using exponential growth (exp-growth) functions.

where P_A and P_O are the output powers or output pulse energies of the laser amplifier and oscillator, respectively, we prefer to define the amplification factor more precisely by:

$$\eta = \frac{P_A/F_A}{P_O/F_O}, \qquad \text{(Equation 4)}$$

and F_A and F_O are the corresponding pump fluence, respectively, since this definition is more reasonably related to the conversion efficiency of the amplifier device. Then, η_A and η are calculated to be about 10 and 3.6, respectively, for the amplifier in Figure S4. Considering the destructive interference between the oscillation and the amplification processes due to the phase difference between them, the amplification factor can still be probably improved. A spacer layer between the DFB microcavity and the HR mirror will help to modify their phase relationship. In such considerations, we insert a PMMA layer with different thickness (S) for regulating the phase shift. The spacer layer introduces an additional phase shift of $\Delta\varphi = 2\pi/\lambda \cdot 2n_{eff}S$, where λ is the wavelength of the injection laser beam and n_{eff} is the effective refractive index of the spacer layer and the grating structure in the normal direction.

For a PMMA layer with S = 257 nm, the output laser properties of the self-injection amplifier are shown in Figure 3. The output laser spectra are plotted in Figure 3A as the pump fluence is increased from 1 to 30.6 μJ/cm^2, where a double-peak lasing line is observed and the two peaks are located at about 580 and 584 nm. The inset of Figure 3A shows an enlarged view of the lasing spectrum at a pump fluence of 30.6 μJ/cm^2 with spectral positions of the two peaks and the dip highlighted by yellow arrows and a red circle. These spectral features can find their precise correspondence in the reflective optical extinction spectrum of the device, as shown in Figure 3B. The optical extinction exhibits a broad valley with it bottom ranging from 580 to 585 nm; however, a small peak was measured at about 582 nm, which is exactly the location of the dip in the lasing spectrum. Therefore, the shape of the lasing spectrum is dominantly controlled by the reflection properties of the HR mirror, verifying the injection locking properties of the laser amplifier.

Figure 3C shows a photograph of the output lasing spot at a distance of about 6 cm from the amplifier device. A bright yellow spot with excellent shape and homogeneity can be observed in the center area. High contrast can be justified for this center spot with respect to the extending "X"-shaped optical field, which is a much improvement when compared with the results in Figures 2 and S4. Furthermore, the whole lasing spectrum shifts to the red with respect to that for the oscillator (Figure 2D) and the amplifier without spacer (Figure S4A). Such a redshift results apparently from the modulation by the optical reflection properties of the HR mirror as a Bragg reflector, which supplies the injection of the amplifier. The modification of the reflection spectrum is controlled by inserting a PMMA spacer layer with a thickness of 257 nm, as shown in Figure 3D. All of above spectral properties evidence the self-injected regenerative amplification properties of the laser device.

Figure 3E shows the measurement of the output laser intensity as a function of the pump fluence. A highest output power of 22 μW, or a pulse energy of 22 nJ, was measured for a pump fluence of 30.6 μJ/cm^2. Using the definition in Equation 1, we may calculate an amplification factor of η_A = 24.4 and η = 13.8 with respect to the oscillator, where η is nearly 4 times as high as the amplifier without a spacer layer. This implies the existence of an optimized thickness of the spacer layer. A most important feature of the relationships in Figure 3E is that an

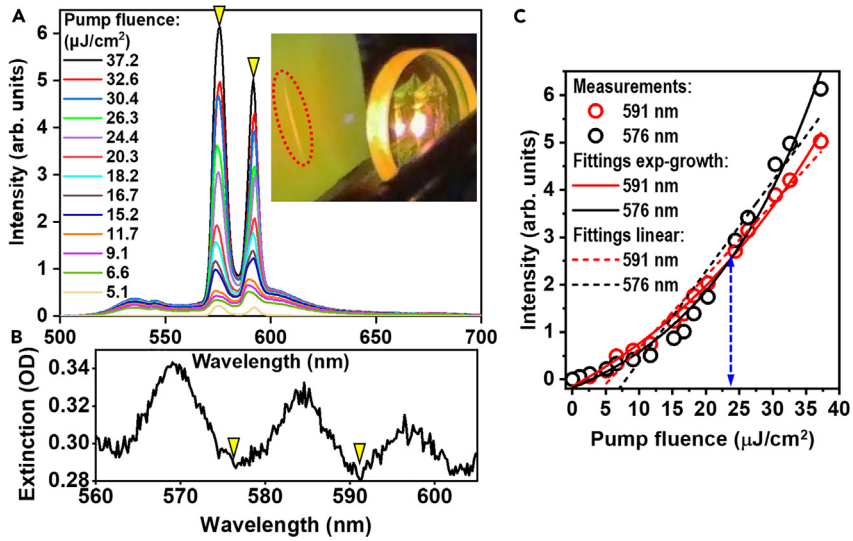

Figure 4. Self-injected regenerative laser amplification for S = 938 nm

(A) Lasing spectra of the self-injected amplifier at different pump fluences. Inset: Photograph of the laser and amplifier device with the output lasing spot.

(B) Reflection optical extinction spectrum measured on the self-injected laser amplifier on a Bragg reflector. The peak and dip features in the lasing spectra may find their correspondence in optical extinction spectrum as highlighted by the yellow triangles.

(C) Measured lasing intensity as a function of pump fluence at about 576 and 591 nm.

exponential growth functions, instead of a linear dependence, is found to fit the measurement data. The peak at 584 nm increases faster than that at 580 nm, corresponding to a higher efficiency. Such an exponential-growth dependence results mainly from the coupling between the oscillation and the amplification processes, where the injection for amplification also takes part in the oscillation before being coupled out, verifying the regenerative amplification nature.

For understanding the exponential growth dependence, we may make a comparison with the conventional two-stage linear fittings. However, we need to be aware that the first linear stage with a low slope corresponds to the variation of the emission before the lasing threshold is reached, and the second corresponds to that after the pump exceeds the threshold. Therefore, we also include the linear fittings to the peak intensities of the lasing spectra at varied pump fluences above the threshold in Figure 3E, as shown by the dashed lines. Apparently, the variations are definitely not linear relationships.

Such an exponential-growth relationship leads to some inconvenience in the precise determination of the pump threshold for the laser device. In this consideration, we show the variation of linewidth as a function of the pump fluence for the emission spectra peaked at 580 and 584 nm in Figures S5A and S5B, respectively. The dramatic change of the linewidth from about 16 nm to 2.4 and 3.7 nm for these two spectral peaks, respectively, justifies a pump threshold between 3.1 and 4.8 $\mu J/cm^2$ for this laser device.

As discussed previously, there exists an optimized thickness of the spacer layer, therefore, it is necessary to determine the optimal value. Thus, we first increase the thickness to S = 436 nm, carried out similar measurements and present the results in Figure S6. In Figure S6A, we show the emission spectra of the device at different pump fluence with the photograph of the lasing spot and the experimental setup included in the inset on the left. Clearly, the amplified lasing output of the amplifier becomes more contrasted from the background and the center lasing spot becomes more isolated from the "X" shaped background, implying enhancement of the amplification process.

Although 4 lasing peaks can be observed at about 570, 577, 583, and 590 nm, only the one at 590 nm shows the best performance, exhibiting a highest intensity and a narrowest bandwidth of about 3 nm at FWHM. The variation of the peak intensity of the lasing spectrum at 590 nm with pump fluence is plotted in the inset of Figure S6A on the right side. Again, an exponential growth function fits the best to the measurement data, agreeing very well with the amplifier inserted with a 257-nm spacer layer. This verifies again the characteristic performance of such a self-injected amplifier by the exponential growth dependence of the output on the input laser energies.

For understanding the mechanism for the 4-peak lasing spectrum, we plot in Figure S6B both the lasing spectrum at a pump fluence of 12.5 $\mu J/cm^2$ and the reflective optical extinction spectrum measured on the device. The 4 lasing peaks basically correspond to the dips of the optical extinction spectrum, as highlighted by the triangles in red and yellow. A highest average power of about 18.6 μW (or a pulse energy of 18.6 nJ) was measured for a pump fluence of about 20.4 $\mu J/cm^2$, corresponding to an amplification factor of $\eta_A \approx 22.6$ and $\eta \approx 17.2$, where the value of η is higher than that for S = 257 nm.

To find out the best design of the injection-locked amplifier, we need to increase further the thickness of the spacer layer. It is understandable that with increasing the thickness of the spacer or the distance between the HR mirror and the DFB resonator, the coherent coupling between the amplifier and the oscillator becomes weaker, so that the output becomes more dominant by the injection-locked amplification of the laser beam. Therefore, when the thickness of the spacer layer is increased to S = 938 nm, an "isolated" laser spot can be observed in the far field, which appears as a bright vertical line, as shown in the inset of Figure 4A, where the X-shaped cross-rings disappeared completely. In

Figure 4A, we show the lasing spectra output from the amplifier at different pump fluence. Two lasing peaks can be observed at about 576 and 591 nm with each having a bandwidth of about 6 nm at FWHM. For determining the mechanisms for the double-peak lasing performance, we show in Figure 4B the reflective optical extinction spectrum of the device. Clearly, the two lasing peaks are exactly located on the two dips of optical extinction, corresponding to stronger injections. Therefore, the amplified laser spectrum is dominantly controlled by the injection, confirming again the regenerative nature of the amplification process. On such basis, the exponential-growth dependence of the output of the amplifier on the pump fluence becomes even stronger, as shown in Figure 4C. The comparison with the linear fittings (dashed lines) supplies clearer evidence.

For completion of the demonstration, we also show in Figure S7 the variation of the bandwidth of the emission spectrum at FWHM with the pump fluence and its comparison with the output intensity for peak wavelengths of 576 and 591 nm. There is clearly a correspondence of the pump threshold with the dramatic narrowing of the output linewidth. This justifies a pump threshold between 2.6 and 5 $\mu J/cm^2$. A maximum output power of 16.2 μW, or a pulse energy of 16.2 nJ, was measured for a pump fluence of 37.2 $\mu J/cm^2$. Thus, an amplification factor of about $\eta_A = 18$ or $\eta = 8.2$ was achieved for S = 934 nm, implying reduced amplification efficiency, as compared with S = 257 and S = 436 nm. However, the best performance should consider both the optical conversion efficiency and the output modes determined by the injection-locking performance. Therefore, an optimized value of the thickness of the spacer layer should be located between 436 and 934 nm.

Conclusions

We report the design of a self-injection-locked regenerative thin-film polymer laser amplifier based on a DFB microcavity combined with a Bragg reflector. Coherent coupling between the HR Bragg mirror and the active DFB resonator constitutes the self-injection and regenerative amplification scheme. A polymeric spacer layer is found crucial for achieving high optical conversion efficiency of the amplification process and high quality of the output laser modes, which not only verifies the injection-locked regenerative amplification process, but also enables optimization of the design of such amplifier devices. The output of the amplifier exhibits a multipeak spectrum, depending strongly on the reflective optical extinction spectrum of the device-covered HR mirror. An exponential-growth dependence, instead of a linear relationship, is found between the output of the amplifier and the pump fluence, which is a further characteristic feature of the self-injection regenerative amplifier. A highest output power of 22 μW, corresponding to a single pulse energy of 22 nJ, and an isolated single laser spot for the transverse mode, have been achieved by optimizing the thickness of the spacer layer. Such an integration scheme enables independent operation of the amplifier, where no additional seeding laser is required for the amplifier. All of these performances imply potentially practical applications of the thin-film polymer laser devices. Furthermore, a metallic film may be used to replace the HR mirror and function both as an optical-feedback/injection device and as an electrode for the electroluminescence devices. Thus, our proposed scheme can be used for exploring electrically pumped organic lasers.

Limitations of the study

Bragg mirrors are used as substrates for the fabrication of the devices. The surfaces of the dielectric film mirrors may be damaged during the fabrication or experimental procedures, which will definitely influence their reflectivity. Furthermore, replacing these mirrors will increase the costs of the experiments. SY-PPV is used as a gain material, but under the long-term irradiation of high-power lasers, it is more prone to photooxidation, so that the lasing performance will degrade. We also need to find a material with strong stability and good luminous properties.

STAR★METHODS

Detailed methods are provided in the online version of this paper and include the following:

- KEY RESOURCES TABLE
- RESOURCE AVAILABILITY
  - Lead contact
  - Materials availability
  - Data and code availability
- EXPERIMENTAL MODEL AND STUDY PARTICIPANT DETAILS
- METHOD DETAILS
  - Experimental procedures
  - Film characterizations
  - Laser amplifier characterizations

SUPPLEMENTAL INFORMATION

Supplemental information can be found online at https://doi.org/10.1016/j.isci.2024.109426.

ACKNOWLEDGMENTS

The authors acknowledge the National Natural Science Foundation of China (12074020).

AUTHOR CONTRIBUTIONS

X.P.Z. designed this research, supervised the experimental work, did the data analysis, and wrote this paper. Y.L. and W.W.W. carried out the optical experiments, microscopic characterization, collected the experimental data, and did the data processing. X.P.Z. supplies all resources for accomplishing this research work.

DECLARATION OF INTERESTS

The authors declare no competing interests.

Received: January 2, 2024
Revised: February 9, 2024
Accepted: March 1, 2024
Published: March 22, 2024

REFERENCES

1. Kuehne, A.J.C., and Gather, M.C. (2016). Organic lasers: recent developments on materials, device geometries, and fabrication techniques. Chem. Rev. *116*, 12823–12864. https://doi.org/10.1021/acs.chemrev.6b00172.
2. Zhang, B.X., Jin, F., Dong, X.Z., Liu, J., and Zheng, M.L. (2022). Switchable lasers via solvent stimulus-responsive photonic crystals. J. Mater. Chem. C *10*, 15075–15083. https://doi.org/10.1039/d2tc01558g.
3. Tessler, N., Denton, G.J., and Friend, R.H. (1996). Lasing from conjugated-polymer microcavities. Nature *382*, 695–697. https://doi.org/10.1038/382695a0.
4. Kozlov, V.G., Bulović, V., Burrows, P.E., and Forrest, S.R. (1997). Laser action in organic semiconductor waveguide and double-heterostructure devices. Nature *389*, 362–364. https://doi.org/10.1038/38693.
5. Yang, S., Wang, Y., and Sun, H. (2015). Advances and prospects for whispering gallery mode microcavities. Adv. Opt. Mater. *3*, 1136–1162. https://doi.org/10.1002/adom.201500232.
6. Toropov, N., Cabello, G., Serrano, M.P., Gutha, R.R., Rafti, M., and Vollmer, F. (2021). Review of biosensing with whispering-gallery mode lasers. Light Sci. Appl. *10*, 42. https://doi.org/10.1038/s41377-021-00471-3.
7. Shi, X.B., Hu, Y., Wang, B., Zhang, L., Wang, Z.K., and Liao, L.S. (2015). Conductive inorganic–organic hybrid distributed bragg reflectors. Adv. Mater. *27*, 6696–6701. https://doi.org/10.1002/adma.201503003.
8. Lidzey, D.G., Bradley, D.D.C., Skolnick, M.S., Virgili, T., Walker, S., and Whittaker, D.M. (1998). Strong exciton–photon coupling in an organic semiconductor microcavity. Nature *395*, 53–55. https://doi.org/10.1038/25692.
9. O'carroll, D., Lieberwirth, I., and Redmond, G. (2007). Microcavity effects and optically pumped lasing in single conjugated polymer nanowires. Nat. Nanotechnol. *2*, 180–184. https://doi.org/10.1038/nnano.2007.35.
10. Senevirathne, C.A.M., Sandanayaka, A.S.D., Karunathilaka, B.S.B., Fujihara, T., Bencheikh, F., Qin, C., Goushi, K., Matsushima, T., and Adachi, C. (2021). Markedly improved performance of optically pumped organic lasers with two-dimensional distributed-feedback gratings. ACS Photonics *8*, 1324–1334. https://doi.org/10.1021/acsphotonics.0c01728.
11. Sandanayaka, A.S.D., Matsushima, T., Bencheikh, F., Yoshida, K., Inoue, M., Fujihara, T., Goushi, K., Ribierre, J.C., and Adachi, C. (2017). Toward continuous-wave operation of organic semiconductor lasers. Sci. Adv. *3*, e1602570. https://doi.org/10.1126/sciadv.1602570.
12. Tsiminis, G., Wang, Y., Kanibolotsky, A.L., Inigo, A.R., Skabara, P.J., Samuel, I.D.W., and Turnbull, G.A. (2013). Nanoimprinted organic semiconductor laser pumped by a light-emitting diode. Adv. Mater. *25*, 2826–2830. https://doi.org/10.1002/adma.201205096.
13. Kuehne, A.J.C., Kaiser, M., Mackintosh, A.R., Wallikewitz, B.H., Hertel, D., Pethrick, R.A., and Meerholz, K. (2011). Sub-micrometer patterning of amorphous-and β-phase in a crosslinkable poly(9,9-dioctylfluorene): dual-wavelength lasing from a mixed-morphology device. Adv. Funct. Mater. *21*, 2564–2570. https://doi.org/10.1002/adfm.201002553.
14. Karl, M., Glackin, J.M.E., Schubert, M., Kronenberg, N.M., Turnbull, G.A., Samuel, I.D.W., and Gather, M.C. (2018). Flexible and ultra-lightweight polymer membrane lasers. Nat. Commun. *9*, 1525. https://doi.org/10.1038/s41467-018-03874-w.
15. Brückner, R., Zakhidov, A.A., Scholz, R., Sudzius, M., Hintschich, S.I., Fröb, H., Lyssenko, V.G., and Leo, K. (2012). Phase-locked coherent modes in a patterned metal–organic microcavity. Nat. Photonics *6*, 322–326. https://doi.org/10.1038/NPHOTON.2012.49.
16. Stehr, J., Crewett, J., Schindler, F., Sperling, R., von Plessen, G., Lemmer, U., Lupton, J.M., Klar, T.A., Feldmann, J., Holleitner, A.W., et al. (2003). A low threshold polymer laser based on metallic nanoparticle gratings. Adv. Mater. *15*, 1726–1729. https://doi.org/10.1002/adma.200305221.
17. Takahashi, S., Ramian, G., and Sherwin, M.S. (2009). Cavity dumping of an injection-locked free-electron laser. Appl. Phys. Lett. *95*, 234102. https://doi.org/10.1063/1.3270041.
18. Ryu, H.Y., Lee, S.H., Kim, E.B., Suh, H.S., and Moon, H.S. (2010). A discretely tunable multifrequency source injection locked to a spectral-mode-filtered fiber laser comb. Appl. Phys. Lett. *97*, 141107. https://doi.org/10.1063/1.3497080.
19. Zhao, X., and Chang-Hasnain, C.J. (2008). A new amplifier model for resonance enhancement of optically injection-locked lasers. IEEE Photon. Technol. Lett. *20*, 395–397. https://doi.org/10.1109/lpt.2008.916911.
20. Snigirev, V., Riedhauser, A., Lihachev, G., Churaev, M., Riemensberger, J., Wang, R.N., Siddharth, A., Huang, G., Möhl, C., Popoff, Y., et al. (2023). Ultrafast tunable lasers using lithium niobate integrated photonics. Nature *615*, 411–417. https://doi.org/10.1038/s41586-023-05724-2.
21. Lihachev, G., Weng, W., Liu, J., Chang, L., Guo, J., He, J., Wang, R.N., Anderson, M.H., Liu, Y., Bowers, J.E., and Kippenberg, T.J. (2022). Platicon microcomb generation using laser self-injection locking. Nat. Commun. *13*, 1771. https://doi.org/10.1038/s41467-022-29431-0.
22. Fragkos, A., Bogris, A., and Syvridis, D. (2013). Efficient orthogonal modulation enabled by injection locked limiting amplifiers. IEEE Photon. Technol. Lett. *25*, 667–670. https://doi.org/10.1109/LPT.2013.2246834.
23. Wang, M., and Zhang, X. (2017). Ultrafast injection-locked amplification in a thin-film distributed feedback microcavity. Nanoscale *9*, 2689–2694. https://doi.org/10.1039/c6nr09973d.
24. Wang, M., and Zhang, X. (2019). Femtosecond tuning dynamics of organic amplifiers based on injection into DFB resonators of slant gratings. Org. Electron. *66*, 156–162. https://doi.org/10.1016/j.orgel.2018.12.032.
25. Wang, M., and Zhang, X. (2019). Femtosecond thin-film laser amplifiers using chirped gratings. ACS Omega *4*, 7980–7986. https://doi.org/10.1021/acsomega.9b00232.

STAR★METHODS

KEY RESOURCES TABLE

REAGENT or RESOURCE	SOURCE	IDENTIFIER
Chemicals, peptides, and recombinant proteins		
SY-PPV	Sigma-Aldrich	900438; CAS:26009-24-5
Positive photoresist	Beijing Tianxing Jian Xingye Technology development Inc	RZJ-304-25
Tetramethylammonium hydroxide	Beijing Bailingwei Technology Inc	999770; CAS:75-59-2
PMMA	Sigma-Aldrich	182265; CAS:9011-14-7
Other		
Bragg high-reflection mirror	China Daheng Group Inc.	GCC-101102

RESOURCE AVAILABILITY

Lead contact

Further information and requests for resources and reagents should be directed to and will be fulfilled by the lead contact, Xinping Zhang (zhangxinping@bjut.edu.cn).

Materials availability

This study did not generate new unique reagents.

Data and code availability

- Data: All data reported in this paper will be shared by the lead contact upon request.
- Code: This paper does not report original code.
- Any additional information required to reanalyze the data reported in this paper is available from the lead contact upon request.

EXPERIMENTAL MODEL AND STUDY PARTICIPANT DETAILS

This work did not need any unique experimental model.

METHOD DETAILS

Experimental procedures

Solution preparation

5.5 mg super yellow was dissolved in 1000 μL methylbenzene solvent and stirred on a hotplate at 50°C for 12 h to prepare a solution with a concentration of 5.5 mg/mL.

Preparation process of self-injection regenerative laser amplifier

In the experiment, a polymethylmethacrylate (PMMA) resist was used for preparing a spacer layer. PMMA dissolved in chlorobenzene was spin coated on the Bragg reflection mirror with the speed of 1000, 2000, 3000 rpm for 30 s, respectively, to produce space layers with different thicknesses.

The sample was then baked on a hotplate (MODELKW-4AH) at 150°C for 3 min in order to evaporate the solvent and to improve the surface quality. The grating structures on top of the spacer layer have been produced by interference lithography, where photoresist (PR) has been exposed to the interference pattern between two UV laser beams. The effective area of the PR grating is about 100 mm^2. The PR was first spin-coated onto the spacer layer at a speed of 2000 rpm. The samples were heated at 110°C for 2 min by a hotplate. Then, the prepared samples were exposed to the interference pattern between two laser beams at 355 nm, where the UV laser source is from COBOLT, Sweden. The period (Λ) of the Bragg grating is determined by $\Lambda = \lambda/(2\sin\theta)$, where λ=355 nm is the wavelength of the UV laser source and θ is the half-angle between the two beams in interference lithography. The period of the gratings was about 345 nm for $\theta = 30.9°$. After being

exposed for 6.9 s and developed for 11 s, the PR Bragg grating was produced. The exposure and development time were adjusted along with various structural parameters. The developed samples were re-heated at 110°C for 2 min by a hotplate. Thereafter, a typical yellow-emitting conjugate polymer (Super Yellow) is chosen as the active material. The solution of Super Yellow in methylbenzene (5.5 mg/ml) is spin-coated onto the Bragg reflector at different speed, producing a self-injection laser amplifiers.

Film characterizations

The SEM images of the distributed feedback microcavities were measured by a scanning electron microscope (JSM-6700F) from JEOL, Tokyo, Japan at an accelerating voltage of 15.0 kV. The thickness of PMMA spacer layer was measured by three-dimensional topography (NanoMap 1000WLI). The absorption spectrum of the super yellow film was measured using the Agilent8453 UV-VIS spectrometer and the PL using a Time Correlated Single Photon Counting system from Edinburgh Instruments.

Laser amplifier characterizations

In characterizing the lasing performance of both the DFB laser and the self-injected amplifier, the frequency doubled Ti:sapphire amplifier is used as the pump source, which supplies laser pulses at 400 nm with a repetition rate of 1 kHz and a pulse length of about 150 fs. The laser spectrum is acquired by an Ocean Optics spectrometer USB 4000 with a resolution of 2 nm. Output laser power is measured using a power-meter from Coherent (PM100D).